Engineering Failure Analysis 61 (2016) 28–36

Contents lists available at ScienceDirect

Engineering Failure Analysis

journal homepage: www.elsevier.com/locate/efa

Analysis of the criticality of flaws found in trunnion of grinding ball mills used in mining plants

M.D.M. Neves *, A.H.P. Andrade, D.N. Silva

IPEN – Instituto de Pesquisas Energéticas e Nucleares, São Paulo, Brazil

ARTICLE INFO

Article history:
Received 1 October 2014
Received in revised form 5 July 2015
Accepted 21 July 2015
Available online 26 July 2015

Keywords:
Flaws
Ball mills
Fracture mechanics

ABSTRACT

The grinding ball mills are equipments present in mining plants, being important in the ore comminution circuits. Depending on numerous factors, such as, for example, inappropriate design, manufacturing, overloads, poor maintenance and inadequate operating procedures, flaws are developed in the structural components of this equipment. The structural components of a mill, basically, shell, heads and trunnions, besides high costs, have lead times that might reach three years, according to market demand. Therefore, it becomes increasingly necessary that any flaws in those components to be properly evaluated. This paper analyzed the fracture mechanics of flaws, such as cracks observed in a ball mill trunnion and compared the theoretical values of growth rate of these defects with actual values obtained through periodic inspections performed in this component. The cracks nucleation was caused by lack of lubrication in the trunnion bearings, generating circumferential thermal stresses, thus the estimated temperature of the trunnion and bushing contact achieved 150 °C. The lack of lubrication was originated by a logic failure which allowed the mill to start and run over the trunnion bearing bushing without the lubrication system to be turned on, that is, without oil film. The logic failure was caused by an operator fault. During the analyzed period, the results obtained by the standard BS7910 proved to be closest to the actual values than the standard ASME, Section XI, Appendix A.

1. Introduction

According to Beraldo [1] comminution of solids is an operation which may be used for many purposes. In the ores beneficiation, comminution is necessary to obtain the granulometry suitable for the concentration process used, as well as to achieve a proper release of the minerals to be separated, that is, in the mining process, the ore is a small percentage of the rock, which is being processed, thus reducing the size of rock of the same ore magnitude will to allow to separate the product to the tailing.

Comminution methods are classified according to the ore granulometry in crushing and grinding, varying the characteristics of the equipments in the two categories of processes [1].

The ball mills are rotary equipment used in mining plants in grinding, which uses steel balls to reduce the particle size of the ore as shown in Fig. 1.

The rotating assembly of the mill is supported by two bearings, called trunnion bearings indicated in Fig. 2. The bearings are static components having bushings, on which the mill rotates. The components of the mill that rotate on bearings are the trunnions. The trunnion is a kind of cylindrical and tubular shaft with thick walls, wherein the ore passes through its inner diameter, both in the feed and in the mill discharge.

* Corresponding author.
E-mail address: mdneves@ipen.br (M.D.M. Neves).

http://dx.doi.org/10.1016/j.engfailanal.2015.07.037
1350-6307/

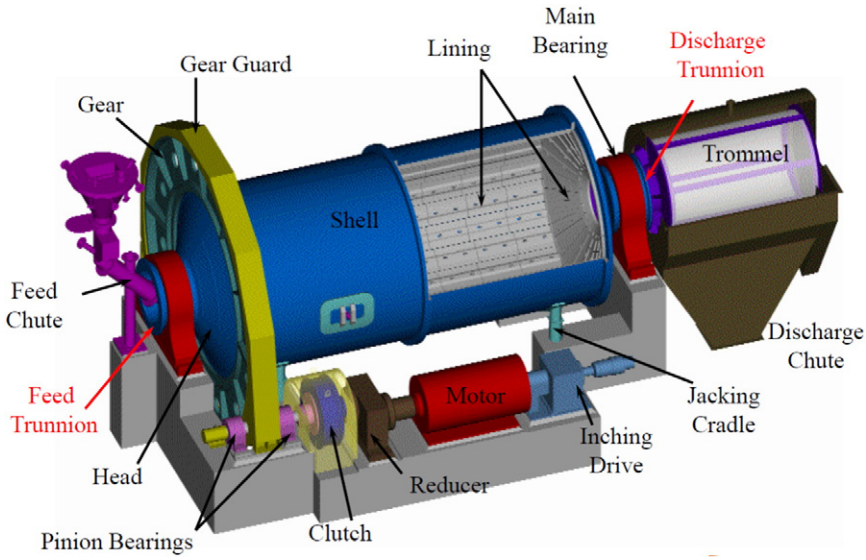

Fig. 1. Schematic representation of ball mill components.

A pressurized oil film prevents metal to metal contact between the trunnion and the bearing bushing and allows the mill to rotate without excessive friction.

1.1. Background

The trunnion analyzed on this present study weighs approximately 28 metric tons and supports more than 1000 t, weight of the mill itself plus the grinding media, ore and water.

Since the trunnion is a component subjected to high loading and responsibility, the appearance of flaws on it is very critical, because if there is a collapse, the entire mining plant may shutdown until a palliative or repair is done or a new part is available. The deadline for making a new trunnion can reach three years depending on the market demand.

The appearance of cracks in a trunnion obligates the plant maintenance to perform periodic monitoring of their growth, that is, the production must be frequently interrupted for such inspection. Mining plants operate 24 h, 365 days per year. Additionally, it is necessary to have a spare trunnion available and the period of repair or replacement of the trunnion is about ten days

The cracks to be analyzed in this study appeared in a trunnion of a ball mill in the region of axial and radial contact with the bearing bushing of the mill. Those cracks were caused by a lack of lubrication, which allowed the metal to metal contact between the trunnion and the bushing. This contact led to a heating in the trunnion, inducing thermal stresses that culminated in the appearance of cracks in various regions of the trunnion.

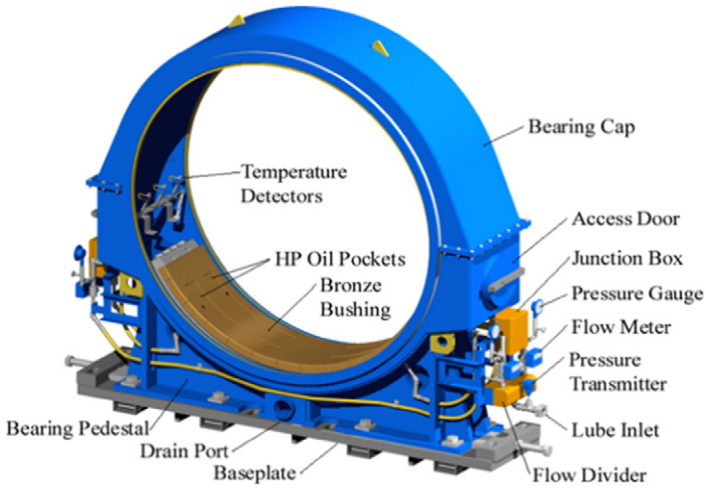

Fig. 2. Trunnion bearing components, including bronze bushing.

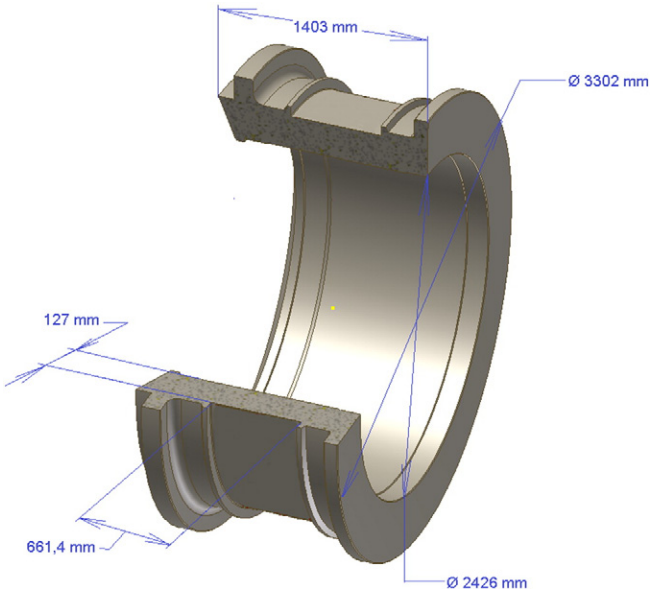

Fig. 3. Trunnion dimension (mm).

It was analyzed the propagation of cracks based on the methodology described in BS7910 [2] and ASME Section XI, Appendix A [3] standards.

2. Experimental

2.1. Trunnion material

This paper was based on a Ø 7.315 m (24 ft) × 12.192 m (40 ft) ball mill used in a typical mining plant. Some basic dimension of the studied trunnion is shown in Fig. 3. The approximate weight is 28 metric tons. The trunnion material was nodular cast iron per DIN 1693 grade GGG-50 [4] equivalent to EN-1563-GJS-500-7 [5]. The bronze bushing dimension is noted in Fig. 4.

2.2. Methods

First of all, it was analyzed the normal operational stresses in the trunnion. Then, it was checked the trunnion and bushing surfaces after the contact among them. After that, it was examined the micrographies of trunnion surfaces.

Thermal stresses were calculated by the use of Strand7 software, version R.2.4.6, according to an estimated temperatures distribution indicated in Fig. 5. This distribution was based on the cracks location at the trunnion shown in Fig. 6 and assuming the most critical cracks

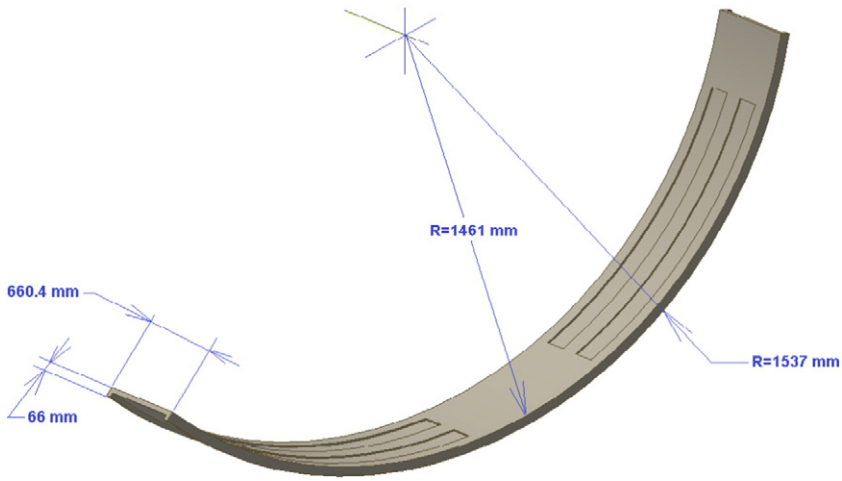

Fig. 4. Bronze bushing dimension.

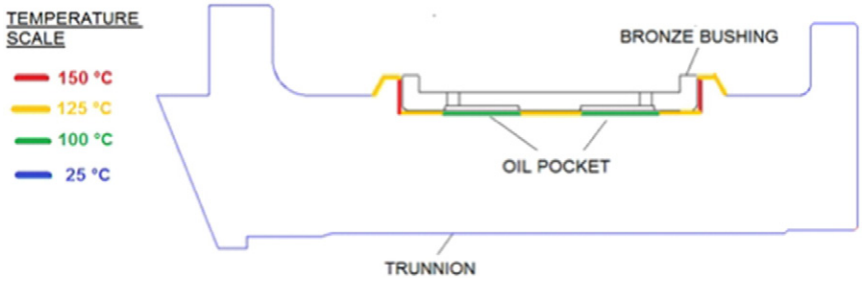

Fig. 5. Surfaces temperatures simulation for thermal stresses.

Fig. 6. Cracks location overview.

were found at the ends of the trunnion shoulder. There is no clearance between the bushing and the trunnion shoulder from an axial direction. Different thermal expansion between the trunnion and the bushing led to higher contact, and consequently heating as assumed in Fig. 5.

The standards BS7910 and ASME Section XI, Appendix A were used to calculate the theoretical crack growth, since there is no specific standard for grinding mill cracks evaluation. The detail of some cracks detected in the trunnion is shown in Fig. 6 and the location of the most critical crack is shown in Fig. 7.

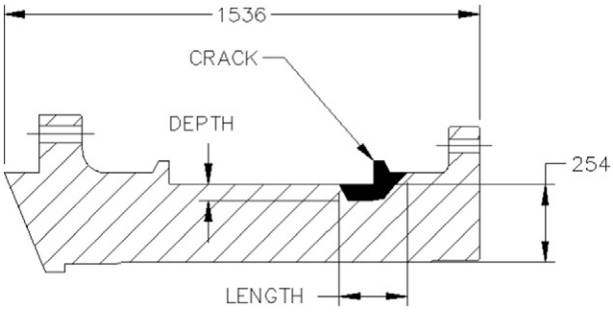

Fig. 7. Location of most critical crack.

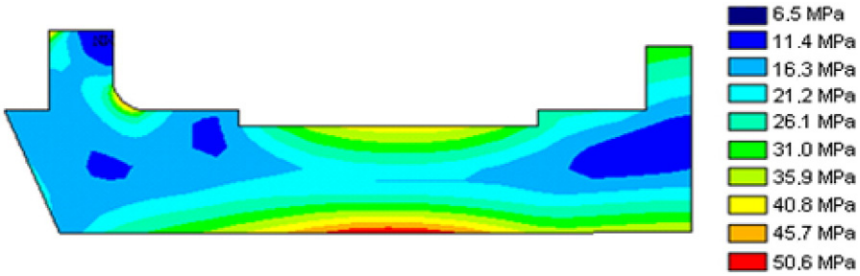

Fig. 8. Trunnion finite element analysis.

Table 1
Trunnion material specification.

Material specification	Results
Yield strength	343 MPa
Tensile strength	616 MPa
Elongation	4%
Hardness	255 HB
% Carbon	3.71–3.73%
% S	0.006–0.006%
% Si	1.98–2.15
% Mn	0.28–0.33%
% P	0.019–0.020%
% Mg	0.039%–0.051%

3. Engineering analysis

Cracks nucleation was related to an incident caused by lack of lubrication which led to a metal–metal contact between the trunnion and the bronze bushing of a hydrostatic bearing. The lack of lubrication was originated by a logic failure which allowed the mill to start and run over the trunnion bearing bushing without the lubrication system to be turned on, that is, without oil film. The logic failure was caused by an operator fault. The maximum trunnion temperature during a normal operation is 57 °C. There is a heat exchange device in the lubrication system that always tries to keep the oil to the mill at 40 °C. The metal–metal contact generates heat, therefore temperature raise and since the lubrication unit was shut down, the root problem was not oil temperature, but oil not reaching the bushing.

Fig. 9. Detail of trunnion marks.

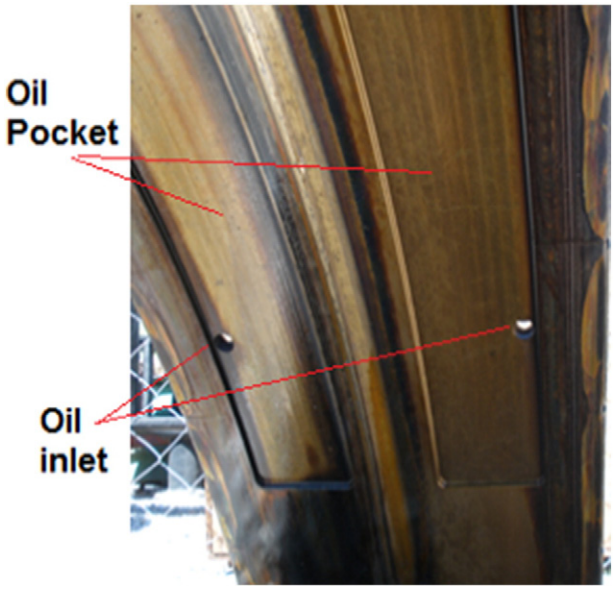

Fig. 10. Detail of bushing marks.

Fig. 8 showed the stress range calculated by Ansys software, version 12.1 for a 30% ball charge, where it was noted that the maximum stress range at the trunnion journal is 40.8 MPa, which was quite below the yield strength indicated in the Table 1. Looking at Fig. 7, considering the location of the most critical size, the stress range at this crack location was even lower, close to 31 MPa. This means there should had not been appeared any crack at this location, called trunnion shoulder, which was supposed to be a low stress region. Moreover, the presence of longitudinal cracks meant the stresses to cause those that were circumferential.

The condition of the trunnion and trunnion bearing bronze bushing immediately after the metal–metal contact are shown in Figs. 9 and 10 respectively. The cracks were not visually detected, however after a dye penetrant test, cracks shown up as indicated in Fig. 6. It was realized there were some dark marks on both components. There were also some light marks which are coincident to oil pockets location, where the oil film is formed, which resulted in less contact between trunnion and bushing, because of residual oil on them. In Fig. 10 it is also shown that the oil inlet holes, where the oil coming from the lubrication system achieved the bushing.

Figs. 11 and 12 showed the micrographies of trunnion surface after the heating caused by lack of lubrication. The light region refers to ferrite phase which involves the dark graphite nodules. The darken areas, which are not the graphite nodules, corresponds to perlite phase, as shown in the literature [6–9].

Fig. 11. Micrography obtained by metallographic replica of trunnion region. Region with light marks from Fig. 7. Zoom 100×.

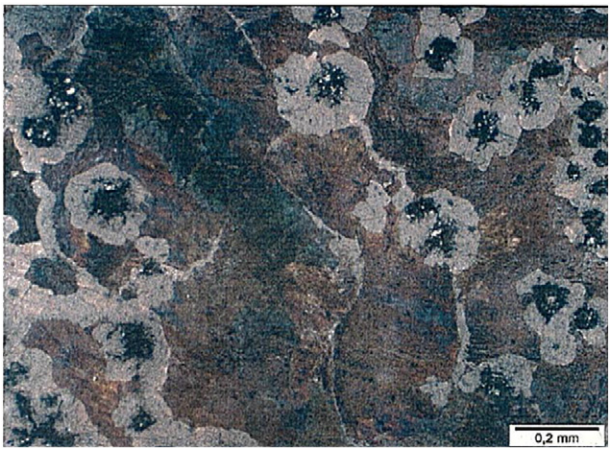

Fig. 12. Micrography obtained by metallographic replica of trunnion region. Region with dark marks from Fig. 7. Zoom 100×.

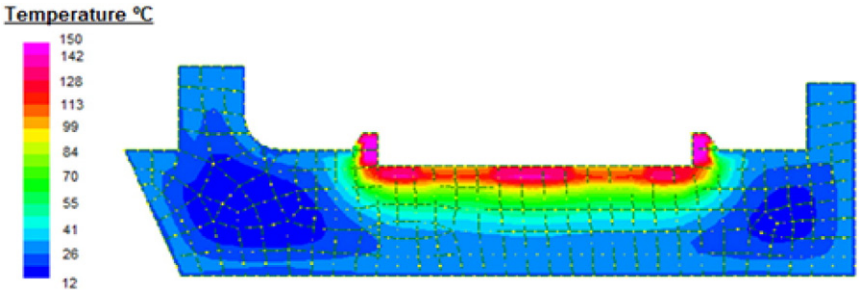

Fig. 13. Temperature gradient distribution.

In Fig. 11 is observed the microstructure of the region from Fig. 9 with light marks, while in Fig. 12 is realized the microstructure of the trunnion region with dark marks from Fig. 9. Note the similarity of both microstructures, indicating that the contact temperature between the trunnion and the bushing did not achieve high values, enough to occur a phase transformation.

The lubrication failure occurred on the feed and discharge trunnion shown in Fig. 1, however the damage severity in the feed trunnion was more critical. This phenomenon is common on mill bearings lubrication failures. The fixed trunnion which is always the trunnion at the side of the drive train is the trunnion which has no gap between it and the bearing bushing. The clearance is all

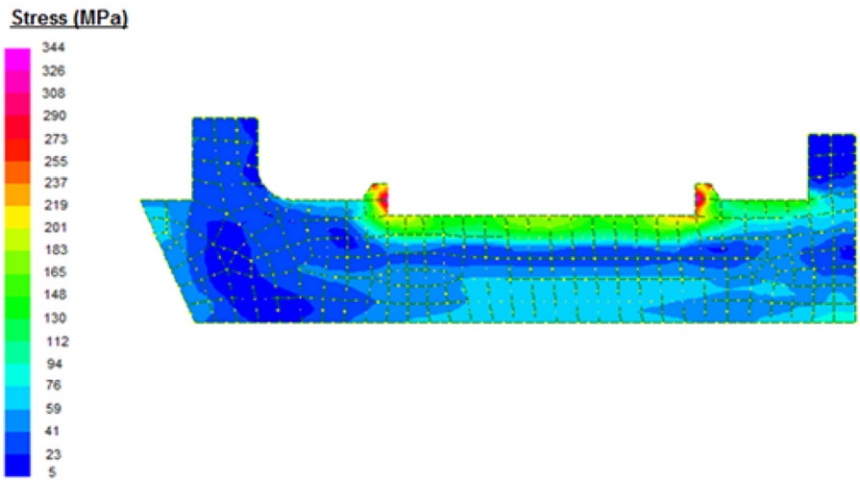

Fig. 14. Stress gradient distribution.

Table 2
Comparison of crack growth actual to theoretical values – BS7910.

Inspection				BS7910			
Days	Cycles	Actual length (mm)	Actual depth (mm)	Ki (MPa* $\sqrt{m}$)	ΔK (MPa* $\sqrt{m}$)	da/dn (m/cycles)	Theoretical depth (mm)
0	0	88	27	7.86	7.86	1.49E-10	27.00
114	2001110	88	27	7.86	7.86	1.49E-10	27.30
335	5880456	88	27	7.86	7.86	1.49E-10	28.17
582	10216195	210	52	11.30	11.30	6.00E-10	34.30
601	10549714	210	52	11.30	11.30	6.00E-10	40.63
617	10830571	210	52	11.30	11.30	6.00E-10	47.13
630	11058768	224	52	11.31	11.31	6.01E-10	53.77
645	11322072	224	52	11.31	11.31	6.01E-10	55.46

transferred to the free trunnion to compensate mill axial thermal expansion. The heat generation for the free trunnion is lessened, mainly due to the axial movement and there is no restriction at the trunnion shoulder to increase it and to cause thermal stresses.

Fig. 13 indicated the temperature through the trunnion cross sectional, based on the methodology considered in Fig. 5 and in the contact marks seen in Figs. 9 and 10. Fig. 14 showed that the thermal stresses distribution along the trunnion where it was observed the maximum stress was 344 MPa, corresponding to a stress higher than yield strength of the material. Therefore, 150 °C at trunnion surface could generate stresses, which combined to the normal duty load were enough to nucleate longitudinal cracks in the trunnion.

Table 2 indicated the measured length and depth obtained by the periodical inspection of the most critical crack. The number of cycles was based on mill speed of 12.19 rpm. According to the standard BS7910 after 645 days, crack size theoretically should have been 55.46 mm and per ASME Section XI, Appendix A, it should have been 71.88 mm. BS7910 standard result was closer to actual depth value and ASME Section XI was more conservative (Table 3).

4. Conclusion

The trunnion surface micrographies prove the contact temperature between the trunnion and the bearing bushing did not achieve high temperature values to cause phase transformation.

Longitudinal cracks detected in low stress areas of the trunnion were caused by thermal stresses, because of lack of oil lubrication between the trunnion and the bushing.

The lack of lubrication was originated by a logic failure which allowed the mill to start and run over the trunnion bearing bushing without the lubrication system to be turned on, that is, without oil film. The logic failure was caused by an operator fault.

A temperature of 150 °C is enough to meet a stress over the yield strength of the material. Therefore, 150 °C at trunnion surface could generate stresses, which combined to the normal duty load were enough to nucleate longitudinal cracks in the trunnion.

The most critical crack growth was evaluated by the use of the standards BS7910 and ASME Section XI, Appendix A, where BS7910 was more accurate and ASME Section XI was more conservative.

It was realized that the theoretical model was adherent to the practical data.

Acknowledgments

For this work we are grateful for the support of IPEN (Instituto de Pesquisas Energéticas e Nucleares).

Table 3
Comparison of crack growth actual to theoretical values - ASME Section XI, Appendix A.

Inspection				ASME Section XI, Appendix A			
Days	Cycles	Actual length (mm)	Actual depth (mm)	Ki (MPa* $\sqrt{m}$)	ΔK (MPa* $\sqrt{m}$)	da/dn (m/cycles)	Theoretical depth (mm)
0	0	88	27	7.64	7.64	1.34E-10	27.00
114	2001110	88	27	7.64	7.64	1.34E-10	27.27
335	5880456	88	27	7.64	7.64	1.34E-10	28.05
582	10216195	210	52	11.20	11.20	5.79E-10	33.97
601	10549714	210	52	11.20	11.20	5.79E-10	40.07
617	10830571	210	52	11.20	11.20	5.79E-10	46.34
630	11058768	224	52	13.37	13.37	1.14E-09	58.96
645	11322072	224	52	13.37	13.37	1.14E-09	71.88

References

[1] BeraldoJ.L. , Moagem de Minérios em Moinhos Tubulares, Pró-Minério/Edgard Blücher, São Paulo 1987, pp. 1–2.
[2] BS7910, Guide to Methods for Assessing the Acceptability of Flaws in Metallic Structures, British Standards Institution, 2005.
[3] ASME, Boiler and Pressure Vessel Code. Section XI, Rules for Inservice Inspection of Nuclear Power Plant Components2010. (Appendix A).
[4] DIN1693, Cast Iron with nodular Graphite Unalloyed and Low Ally Grades, Deutsche Normen, 1973.
[5] BS EN, Founding – spheroidal graphite cast irons, Annex F 34–37 (1563-2011) 34–37.
[6] ASM metals handbook, Properties and Selection: Iron. Steels and High Performance Alloys, 10th Edition, 1, 1994.
[7] E.N. Pan, et al., High Temperature Thermal Fatigue Property of Thin-Section Ductile Cast Iron, American Foundry Society, Schaumburg. IL, 2010.
[8] LarkerR. , Solution strengthened ferritic ductile iron ISO 1083/JS/500/10 provides superior consistent properties in hydraulic rotators, 2008 Keith Millis Symposium on Ductile Cast Iron. American. Las Vegas, 2008.
[9] F. Unkic, et al., The influence of elevated temperatures on microstructure of cast irons for automotive engine thermo-mechanical loaded parts, RMZ – Mater. Geoenviron. Vol. 56 (N° 1) (2009) 9–23.